ON THE MICRO-STRUCTURE OF THE SCALAR FIELD IN COMPRESSIBLE FORCED ISOTROPIC TURBULENCE AND SUPERSONIC CHANNEL FLOW

Holger Foysi, Rainer Friedrich
Fachgebiet Stroemungsmechanik,
Technische Universitaet Muenchen,
Boltzmannstr. 15, D-85748 Garching, GERMANY
holger@flm.mw.tu-muenchen.de
R.Friedrich@lrz.tu-muenchen.de

Sutanu Sarkar
Department of Aerospace Engineering,
Univ. of California San Diego
9500 Gilman Drive, La Jolla, CA 92093-0411, USA
sarkar@uscd.edu

ABSTRACT

The present work investigates the influence of compressibility on the fluctuating gradient of a passive scalar, its alignment with the principal directions of strain and the topology of the scalar gradient field. Two flows are considered: forced isotropic turbulence and supersonic channel flow. The turbulent Mach numbers of the isotropic field are between $M_t = 0.05$ and $M_t = 0.63$. The Taylor Reynolds number is $Re_\lambda \approx 50$. A mean scalar gradient is prescribed. The turbulent supersonic channel flow data result from four simulations with Reynolds numbers based on the friction velocity of $Re_\tau = 180$ up to $Re_\tau = 1030$ and bulk Mach numbers ranging from $M = 0.3$ up to $M = 3.5$. It is shown that the scalar gradient alignment is hardly changed by compressibility, even in the vicinity of a wall, where variable property effects are important. The production of the absolute value of the scalar gradient is slightly reduced, along with the production of enstrophy due to vortex stretching.

INTRODUCTION

The microstructure of a passive scalar field, especially the alignment of the scalar gradient with the principal directions of strain, has been investigated in detail in incompressible homogeneous, turbulent flow (e.g. Ashurst et al. (1987), Brethouwer et al. (2003)). There it was found, that the scalar gradient tends to align with the eigenvector of the strain rate tensor corresponding to the compressive principal axis. The topology of the scalar field was shown to be mostly sheet like, which can be seen by conditioning the scalar gradient on the invariants of the velocity gradient tensor. Large values of the scalar gradient, conditioned on the second and third invariants, were seen in the fourth quadrant corresponding to one compressive and two extensional directions (Brethouwer et al. (2003)). On the other hand it was seen, that the scalar gradient was small in vorticity dominated regions. It is well known that the vorticity vector in incompressible flow is generally aligned with the eigenvector of the strain tensor associated to the intermediate eigenvalue (Vincent and Meneguzzi (1991), Dresselhaus and Tabor (1991)). Recent results of compressible decaying isotropic turbulence (Erlebacher and Sarkar (1993), Pirozzoli and Grasso (2004)) report similar findings, with a small decrease of the eigenvalues resulting in a decreased production of the enstrophy due to vortex stretching.

Fall	$\mathbf{M_t}$	$\mathbf{Re_\lambda}$	$\frac{\mathbf{L_{x_i}}}{\pi}$	$\mathbf{N_i}$	L_I/L_{x_i}	$\mathfrak{g}$
M1	0.05	51	0.01	128	0.46	1.0
M2	0.1	55	0.01	128	0.47	1.0
M3	0.15	56	0.01	128	0.48	1.0
M4	0.22	58	0.01	128	0.49	1.0
M5	0.34	49	0.01	256	0.43	1.0
M6	0.63	47	0.01	256	0.39	1.0

Table 1: Parameters of the DNS of forced isotropic turbulence.

In the present work we raise the questions: What is the influence of compressibility on the microstructure of a scalar field in homogeneous and inhomogeneous flows? How is the scalar gradient alignment influenced by strong temperature and density gradients or by intrinsic compressibility effects? The present paper is organized as follows. First a short overview of the direct numerical simulations is given. Based on the incompressible analysis of Brethouwer et al. (2003), transport equations for the absolute value of the fluctuating scalar gradient and its alignment with the principle directions of strain are reported. To assess the influence of the different terms in these transport equations, conditional expectations and probability density functions have been calculated. Some of these quantities, obtained from the direct numerical simulations, are discussed in the last section .

NUMERICAL METHOD

Direct numerical simulations of forced compressible isotropic turbulence and supersonic channel flow have been performed. The Navier-Stokes equations and a passive scalar transport equation were discretized using 6th order compact central schemes for the spatial derivatives and a third order low-storage Runge-Kutta scheme for time integration. The primitive variables were filtered after each timestep using a sixth order compact filter to prevent spurious accumulation of energy in the highest wavenumbers.

Forced compressible isotropic turbulence was simulated at a Taylor microscale Reynolds number of approximately 50 and

Case	M	Re_τ	$\frac{L_{x1}}{h}$	$\frac{L_{x2}}{h}$	$\frac{L_{x3}}{h}$	N_{x1}	N_{x2}	N_{x3}
M0.3	0.3	181	9.6h	6h	2h	192	160	129
M1.5	1.5	221	4πh	$\frac{4\pi}{3}$h	2h	192	128	151
M3.0	3.0	560	4πh	$\frac{4\pi}{3}$h	2h	512	256	221
M3.5	3.5	1030	6πh	2πh	2h	512	256	301

Table 2: Parameters of supersonic channel DNS.

turbulence Mach numbers ranging from $M_t = 0.05$ up to $M_t = 0.6$ (where $M_t = \sqrt{\overline{u_1^2 + u_2^2 + u_3^2}}/\bar{c}$). Table 1 contains the simulation parameters.

The isotropic turbulence simulations were forced in physical space to avoid any dependence on the initial conditions, using a combination of sine and cosine functions with random phases, such that only the solenoidal part of the velocity is forced. Since, in compressible isotropic turbulence, the energy injection through the forcing is converted via viscous dissipation into internal energy and therefore causes the instantaneous temperature and pressure to increase in time, a heat sink term was added to the pressure and entropy equation, to guarantee statistically steady values for the pressure and temperature and as a consequence for the Reynolds and Mach numbers. A mean scalar gradient $\mathfrak{g}$ in the x_3-direction was prescribed and the scalar was injected after the turbulence reached a statistically steady state.

The main advantage of the forcing mechanism used here compared to that of other authors (e.g. Kida and Orszag (1990), Lou and Miller (2001)) is the ability to take long time averages at constant Mach and Reynolds numbers and to be independent of the initial conditions.

DNS of supersonic channel flow at $\mathrm{Re}_\tau = 221$ had been done previously by Coleman et al. (1995) and Lechner (2001). Foysi et al. (2004) simulated Reynolds numbers up to $Re_\tau = 1030$. Here, we use the DNS database of Foysi et al. (2004) to investigate variable property effects on the scalar gradient and its alignment.

Some important parameters of the supersonic channel flow can be seen in table 2. The bulk Mach numbers range from $M = 0.3$ to $M = 3.5$ and the friction Reynolds numbers go up to $Re_\tau = 1030$. The simulations are performed to predict turbulent, supersonic channel flow between isothermal walls and transport of a passive scalar introduced from one side and removed from the other. The bulk density and velocity ρ_m, u_m and wall temperature T_w are held constant. These quantities and the channel half-width h are used to define the Mach number $M = u_m/c_w$ and the Reynolds number $\mathrm{Re} = \rho_m u_m h/\mu_w$. $\mathrm{Re}_\tau = \rho_w u_\tau h/\mu_w$ is the Reynolds number based on the friction velocity $u_\tau = (\tau_w/\rho_w)^{1/2}$. It is a result of the computation. To enforce streamwise periodic boundary conditions in the simulation, the mean pressure gradient $-\partial\overline{p}/\partial x$ has been replaced by a body force of type $\overline{f}$. In the course of the simulation the body force $\overline{f}$ is controlled to achieve constant mass flux. At time level n it is therefore calculated as

$$\bar{f} = \frac{\{\overline{\rho u_1}\}^0 - \{\overline{\rho u_1}\}^n}{\Delta t} + \frac{\overline{\tau_{12}}}{h} \qquad (1)$$

A mean scalar gradient is imposed on the flow, using an initial profile of the form (Johansson and Wikström (1999))

$$\theta(x_1, x_2, x_3) = log_{10}\left\{\frac{y_o + x_2}{y_o - x_2}\right\} / \left\{\frac{y_o + 1}{y_o - 1}\right\}, \quad y_o = 1.007 \quad (2)$$

and the boundary conditions $\theta(x_1/h, 0, x_3/h, t) = 1$ and $\theta(x_1/h, 2, x_3/h, t) = -1$.

RESULTS

Transport equations

To investigate the influence of compressibility on the scalar gradient and its alignment, following the procedure of Dresselhaus and Tabor (1991) and Brethouwer et al. (2003) for incompressible flow, equations for the magnitude g of the fluctuating scalar gradient $\mathbf{g}$ and the alignment $\lambda_i = \langle \mathbf{n}, \mathbf{e}_i \rangle$ of the fluctuating unit vector $\mathbf{n} = \mathbf{g}/g$ with the principal directions of strain $\mathbf{e}_i$ (the i^{th} eigenvector of the rate-of-strain tensor $\mathbf{S}$) have been derived. These equations read (for details refer to Foysi (2005))

$$\begin{aligned}
\frac{1}{g}\frac{dg}{dt} = & - s_i\lambda_i^2 - \frac{1}{g^2}\langle \mathfrak{g}, \mathbf{S}\mathbf{g}\rangle - \frac{1}{2g^2}\langle \mathbf{g}, \mathfrak{g}\times\boldsymbol{\omega}\rangle \\
& + \frac{1}{2g^2}(D\Delta g^2 - 2D\boldsymbol{\nabla}\mathbf{g} : \boldsymbol{\nabla}\mathbf{g}) \\
& - \frac{1}{\rho^2}\left\langle \frac{\mathbf{g}}{g}, \boldsymbol{\nabla}\rho \right\rangle \left\langle \boldsymbol{\nabla}(\rho D), \frac{\mathbf{g}}{g} \right\rangle \\
& + \frac{1}{\rho}\left\langle \frac{\mathbf{g}}{g}, \left\{ \left\langle \frac{\mathbf{g}}{g}, \boldsymbol{\nabla} \right\rangle \boldsymbol{\nabla}(\rho D) \right\} \right\rangle \\
& + \frac{1}{\rho}\left\langle \frac{\mathbf{g}}{g^2}, \langle \boldsymbol{\nabla}(\rho D), \boldsymbol{\nabla}\rangle \mathbf{g} \right\rangle + \left\langle \frac{\mathbf{g}}{g^2}, \boldsymbol{\nabla} D \right\rangle \langle \boldsymbol{\nabla}, \mathbf{g}\rangle \\
& + \left\langle \frac{\mathbf{g}}{\rho g^2}, \boldsymbol{\nabla}\{\langle \boldsymbol{\nabla}, \rho D\mathfrak{g}\rangle\} \right\rangle - \frac{\langle \mathbf{g}, \boldsymbol{\nabla}\rho\rangle}{(g\rho)^2}\langle \mathfrak{g}, \boldsymbol{\nabla}\rangle(\rho D), \qquad (3)
\end{aligned}$$

and (terms containing $|\mathfrak{g}|/g$ are small and have been neglected)

$$\begin{aligned}
\frac{d\boldsymbol{\lambda}}{dt} = & \underbrace{-\begin{pmatrix} s_\alpha & 0 & 0 \\ 0 & s_\beta & 0 \\ 0 & 0 & s_\gamma \end{pmatrix}\boldsymbol{\lambda} + (s_i\lambda_i^2\mathbf{I})\boldsymbol{\lambda}}_{\mathbf{c}} + (\frac{\boldsymbol{\omega}}{2} - \boldsymbol{\Omega}')\times\boldsymbol{\lambda} \\
& + \mathbf{E}[\mathbf{I} - \mathbf{n}\otimes\mathbf{n}]\left(D\frac{\Delta\mathbf{g}}{g}\right) - \mathbf{E}[\mathbf{I} - \mathbf{n}\otimes\mathbf{n}]\boldsymbol{\sigma}, \qquad (4)
\end{aligned}$$

with

$$\begin{aligned}
\boldsymbol{\sigma} = & - \frac{\boldsymbol{\nabla}\rho}{\rho^2}\langle \boldsymbol{\nabla}(\rho D), \mathbf{g}\rangle + \frac{1}{\rho}\langle \mathbf{g}, \boldsymbol{\nabla}\rangle\boldsymbol{\nabla}(\rho D) + \frac{1}{\rho}\langle \boldsymbol{\nabla}(\rho D), \boldsymbol{\nabla}\rangle\mathbf{g} \\
& + (\boldsymbol{\nabla} D)\langle \boldsymbol{\nabla}, \mathbf{g}\rangle - \frac{\boldsymbol{\nabla}\rho}{\rho^2}\langle \boldsymbol{\nabla}, \rho D\mathfrak{g}\rangle + \frac{1}{\rho}\langle \mathfrak{g}, \boldsymbol{\nabla}\rangle\boldsymbol{\nabla}(\rho D). \qquad (5)
\end{aligned}$$

D is the diffusivity of the scalar, s_i are the eigenvalues of the strain rate tensor and E is a matrix with the orthonormalized eigenvectors as rows. $\mathfrak{g}$ denotes the prescribed mean scalar gradient in isotropic turbulence and the mean wall normal scalar gradient in supersonic channel flow (the other components are zero due to homogeneity). $\langle\cdot,\cdot\rangle$ denotes the scalar product. In incompressible flow the incompressibility constraint guarantees that one eigenvalue is always negative, corresponding to the most compressive strain direction, one is always positive whereas the intermediate one is mostly positive (Dresselhaus and Tabor (1991)). In the following, the eigenvalues are ordered in the form $s_1 \le s_2 \le s_3$. The terms in the first line of equation (3) represent production terms due to the rate of strain, the mean scalar gradient and the vorticity. The second term in the second row is a molecular destruction term whereas the terms in the remaining four lines indicate the explicit influence of compressiblity due to density and diffusivity gradients. An order of magnitude analysis shows that the first term on the rhs is probably the most important one and depends explicitly on the orientation of the scalar gradient with respect to the principle axes of strain. If, as in the incompressible case, the scalar gradient aligns mostly with $\mathbf{e}_1$, this term

gives a positive contribution and tends to increase the scalar gradient. The compressibility terms can, on the other hand, be important if large mean property variations occur, as in the vicinity of cooled walls or in combustion problems. Equation (4) shows how the alignment of the scalar gradient is affected by strain (first two terms on the rhs), vorticity and rotation of the eigenvectors (third term), molecular diffusion (penultimative term) and compressibility (last term). In Brethouwer et al. (2003) and Foysi (2005) it is discussed in detail how strain and vorticity influence the alignment of the scalar gradient. However it is interesting to assess the influence of the last term on the alignment of $\mathbf{g}$, especially in supersonic channel flow where large density and viscosity gradients occur near the wall. Since the wall normal gradients in the vicinity of the wall are dominant, we have $\sigma_2 \gg \sigma_1, \sigma_3$ and $n_2 \gg n_1, n_3$ with $n_2 \approx 1$ near the wall. Thus, $\mathbf{E}(\mathbf{I} - \mathbf{n} \otimes \mathbf{n})\boldsymbol{\sigma}$ can be approximated by $(1 - n_2^2)((\mathbf{e}_1)_2, (\mathbf{e}_2)_2, (\mathbf{e}_3)_2)$, which is small for $x_2^+ < 70$. The scalar gradient alignment should therefore be nearly independent of the mean property variation in the supersonic channel.

A further investigation of the above equations shows (Foysi (2005)), that the angle formed by the scalar gradient and $\mathbf{e}_1$ should be 45 degrees near the wall and approach a perfect alignment with $\mathbf{e}_1$ in the channel core, where the turbulence is nearly isotropic. Since the wall normal gradients outweight the gradients in the homogeneous directions, there should be a similiar dependence of the scalar gradient on the vorticity, as is generally observed with respect to the strain rate, contrary to isotropic flow.

Isotropic turbulence

Figures 1a and 1b show the scalar gradient, conditioned on the solenoidal (s^I) and compressible part (s^C) of the strain rate $s = \sqrt{S_{ij}S_{ij}}$, obtained after performing a Helmholtz decomposition of the velocity field (the superscript 'C' hereafter indicates the compressible part, the index 'I' the incompressible part). As in the incompressible case, (Brethouwer et al. (2003)) there is a high probability for large scalar gradients to occur in regions with a high strain rate s^I. Conditioned on the compressible part s^C, on the other hand, there is no dependency of $\mathbf{g}$ on s^C visible for case M6. For the compressible part, instead of being aligned with the direction associated with the compressive strain (Figure 2a shows that there is a high probabilty for $\mathbf{g}$ to be aligned with the eigenvector $\mathbf{e}_1^I$), $\mathbf{g}$ tends to be aligned with $\mathbf{e}_3^C$, the eigenvector corresponding to the largest positive eigenvalue. This results in a negative contribution to the production term, $-s_i^C(\lambda^C)^2$, rendering the scalar gradient independent of the compressible part of the strain rate.

Figure 3a shows the scalar gradient conditioned on the vorticity. As is clearly seen, we have strong scalar gradients in regions only, where the vorticity is small. The alignment of the vorticity vector itself is found to be in the direction of $\mathbf{e}_2$ as seen, too, by Pirozzoli and Grasso (2004) (Figure 3b). Compressibility, therefore, does not alter the findings, made in the incompressible case (Brethouwer et al. (2003)). Figures 4a and 4b give an impression of the direct effect of compressibility on the magnitude of the scalar gradient. Here, the scalar gradient conditioned on the density and viscosity gradient is shown. One clearly observes a direct influence of the density and viscosity on g, leading to strong scalar gradients in regions with strong density and viscosity gradients.

Overall it was observed (Foysi (2005)), that the effect of compressibility on the alignment of $\mathbf{g}$ with the principle axes was small. Differences showed up only in the tails of the pdf, increasing the probability of an alignment of $\mathbf{g}$ with $\mathbf{e}_2$. In agreement with the simulations of Pirozzoli and Grasso (2004), a slight decrease of the mean of the rate of strain eigenvalues is observed, with increasing M_t. As a consequence, the production term $-s_i\lambda_i^2$ and the production term due to vortex stretching in the enstrophy budget, which can be written as $-s_i\langle\omega, e_i\rangle^2$, decrease. This leads to decreased scalar gradients and enstrophy in compressible flow.

Supersonic channel flow

If the channel flow is assumed to behave like a simple shear flow in the vicinity of the wall, a short analysis of equations (3) and (4) leads to an angle of 45 degrees between $\mathbf{e}_1$, $\mathbf{e}_3$ and $\mathbf{g}$. In the channel core, a similar behavior like for the isotropic turbulence can be expected. Figures 5a and 5b show the alignment of $\mathbf{g}$ with $\mathbf{e}_1$ at $x_2^+ \approx 6$ and at the channel centre. As expected we find values of $\pm\frac{\sqrt{2}}{2}$ for the cosine of $\langle\mathbf{n}, \mathbf{e}_1\rangle$ (the same is also true with respect to $\mathbf{e}_3$, not shown here). As shown above, there is nearly no influence of the strong variable property effect on the alignment. Although these results imply, that compressiblity effects on the alignment of $\mathbf{g}$ in wall bounded flows of this type have not to be considered. Models which are based on the assumption of an alignment of the scalar gradient in the direction of $\mathbf{e}_1$ (e.g. Peters and Trouillet (2002)) have to account for the change of the alignment of $\mathbf{g}$ when approaching the wall.

Figures 6 and 7 show the scalar gradient conditioned on the strain rate and the vorticity, respectively, at $x_2^+ \approx 6$ and at the channel centre. In the channel core, a similiar behaviour as in isotropic turbulence is observed (figures 6b and 6c), namely large scalar gradients in regions of high strain and low vorticity. Because of the dominance of the wall normal gradients, contrary to the isotropic turbulence, the vorticity is dominated by gradients of the form $\frac{\partial u_i}{\partial x_2}$ and influences $\mathbf{g}$ in a similar way as the strain rate in the near wall region. For the conditional expectations of the scalar gradient it was found, that the differences in the curves, occuring for different Mach numbers, are caused through variable property effects. Normalizing the conditional expectations with semi-local scalings in the near wall region (see Foysi et al. (2004)) leads to a collapse of the curves for different Mach and Reynolds numbers. This is clearly shown in figures 6a and 7a.

Topology of the passive scalar field in isotropic turbulence

In order to investigate the connection between the scalar gradient and the flow topology, the procedure and classification developed by Chong et al. (1990) was adopted for the case of isotropic turbulence. It is interesting to see whether the sheet like structure of the scalar field, which was observed in incompressible flow (e.g. Brethouwer et al. (2003)), is changed with increasing Mach number. The flow topology is described by analyzing the eigenvalues of the velocity gradient tensor $A_{ij} = \frac{\partial u_i}{\partial x_j}$ together with its invariants

$$\begin{aligned} D &= -A_{ii} \\ Q &= -\frac{1}{2}A_{ij}A_{ji} = \frac{1}{4}\omega_i\omega_i - \frac{1}{2}s_{ij}s_{ij} \\ R &= -\frac{1}{3}A_{ij}A_{jk}A_{ki}. \end{aligned} \tag{6}$$

Compared to incompressible flow, the first invariant is not zero, but sufficiently small here, to allow for a similiar classification. In figures 8a and 8b, the scalar gradient conditioned on Q and R for $D=0$ is shown, for cases M1 and M6, respectively. The results usually change with increasing magnitude of the dilatation, showing conditional expectations which get focused stronger around $P=Q=0$. In the plots, the curved line indicates the discriminant of $\mathbf{A}$, which separates complex from real solutions. If $R<0$ the structures are often described as 'cigar'-like, whereas if $R>0$ the structures are 'pancake'-like. The scalar gradient conditioned on Q and R shows the typical 'teardrop shape' as observed before (Brethouwer et al. (2003), Pirozzoli and Grasso (2004)), with the highest values found in the fourth quadrant, corresponding to one direction of compression and two extensional directions. With increasing M_t however, an increased probability is observed, to find large values of the scalar gradient in the second quadrant (two directions of compression and one extensional direction, i.e. a stable focus stretching topology). With increasing Mach number the ramp cliff structure, which is typically observed in scalar fields, seems therefore to be slightly smoothed. This was indeed observed (Foysi (2005)) in contour plots of the passive scalar field.

CONCLUSIONS

To assess the incluence of compressiblity on the microstructure of the passive scalar field, the dependence of the scalar gradient on strain, vorticity and variable property gradients has been investigated. This was done through a derivation of transport equations for the magnitude of the fluctuating scalar gradient and its alignment with the principle directions of strain. Based on two reference flows, conditional expectations and probability density functions were calculated to analyse the importance of the various terms in the transport equations.

Supersonic channel flow at various Mach numbers was considered, to investigate the effect of a wall boundary condition and the strong variable property effects on the scalar gradient. It can be seen from the transport equation for $\boldsymbol{\lambda}$, that the influence of compressibility near the wall on the scalar gradient alignment is negligible, which is confirmed by the DNS results. Differences between the conditional expectations of the scalar gradient are due to variable property effects, because the curves collapse when normalized with a semi-local scaling.

In addition to the channel flow, forced isotropic turbulence at various turbulent Mach numbers is condidered to study intrinsic compressibility effects on the passive scalar microstructure. Larger changes were only observed for the case with the highest Mach number ($M_t = 0.63$). It is seen, that the scalar gradient is aligned with the eigenvector associated to the compressive strain direction, if the solenoidal part of the strain rate tensor is taken and $\mathbf{g}$ is aligned with the eigenvector associated to the largest positive eigenvalue, if the rotation free part of S_{ij} is taken. This gives a negative contribution to the dominant production term in the transport equation for g. A slight reduction of the eigenvalues with increasing Mach number is observed (as in Pirozzoli and Grasso (2004)), which causes a decrease of the scalar gradient production and the production of the enstrophy due to vortex stretching.

Furthermore it was observed, that with higher Mach number the preference for scalar gradients to occur in regions with a stable focus stretching topology, increases.

REFERENCES

Ashurst, W., Kerstein, A., Kerr, R., and Gibson, C. (1987). Alignment of vorticity and scalar gradient with strain rate in simulated Navier-Stokes turbulence. *Phys. Fluids*, 30:2343–2353.

Brethouwer, G., Hunt, J., and Nieuwstadt, F. (2003). Microstructure and Lagrangian statistics of the scalar field with a mean gradient in isotropic turbulence. *Journal of Flud. Mech.*, 474:193–225.

Chong, S., Perry, A. E., and Cantwell, B. (1990). A general classification of threedimensional flow fields. *Phys. Fluids A*, 2:765–.

Coleman, G., Kim, J., and Moser, R. (1995). Turbulent supersonic isothermal-wall channel flow. *J. Fluid Mech.*, 305:159–183.

Dresselhaus, E. and Tabor, M. (1991). The kinematics of stretching and alignment of material elements in general flow fields. *Journal of Flud. Mech.*, 236:415–444.

Erlebacher, G. and Sarkar, S. (1993). Statistical Analysis of the rate of strain tensor in compressible Homogeneous Turbulence. *Phys. Fluids A*, 5:3240–3254.

Foysi, H. (2005). *Transport passiver Skalare in wandgebundener und isotroper kompressibler Turbulenz*. Dissertation, TU München.

Foysi, H., Sarkar, S., and Friedrich, R. (2004). Compressibility Effects and Turbulence Scalings in Supersonic Channel Flow. *J. Fluid Mech.*, 509:207–216.

Johansson, A. V. and Wikström, P. M. (1999). DNS and Modelling of Passive Scalar Transport in Turbulent Channel Flow with a Focus on Scalar Dissipation Rate Modelling. *Flow, Turbulence and Combustion*, 63:223–245.

Kida, S. and Orszag, S. (1990). Energy and Spectral Dynamics in Forced Compressible Turbulence. *J. of Scientific Comp.*, 5:85–125.

Lechner, R. B. (2001). *Kompressible turbulente Kanalströmungen*. VDI Verlag.

Lou, H. and Miller, R. S. (2001). On the scalar probability density function transport equation for binary mixing in isotropic turbulence. *Phys. Fluids*, 13(11):3386–3399.

Peters, N. and Trouillet, P. (2002). On the Role of Quasi-one-dimensional Dissipation Layers in Turbulent Scalar Mixing. *Center of Turbulence Research, Stanford*.

Pirozzoli, S. and Grasso, F. (2004). Direct numerical simulations of isotropic compressible turbulence: Influence of compressibility on dynamics and structures. *Phys. Fluids*, 16(12):4386–.

Vincent, A. and Meneguzzi, M. (1991). The spatial structure and statistical properties of homogeneous turbulence. *J. Fluid Mech.*, 225:1–20.

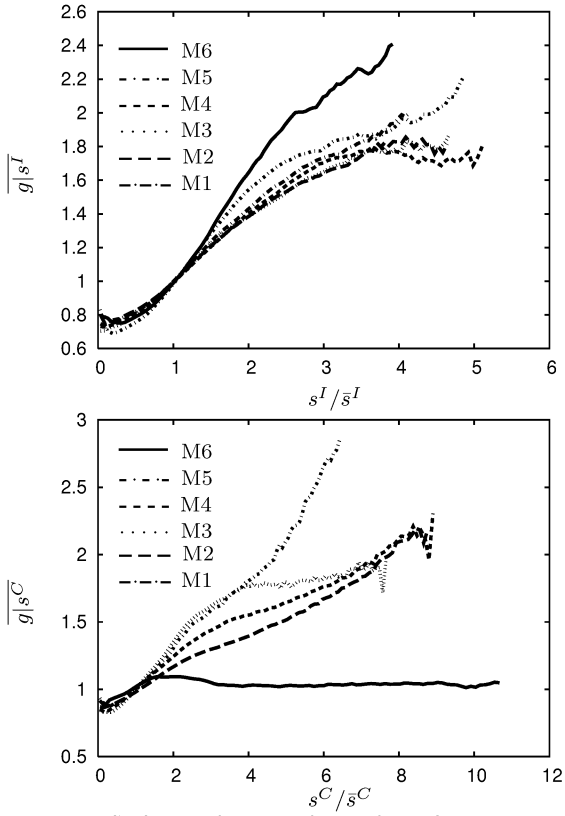

Figure 1: Scalar gradient conditioned on the incompressible (a) and compressible part (b) of the strain rate.

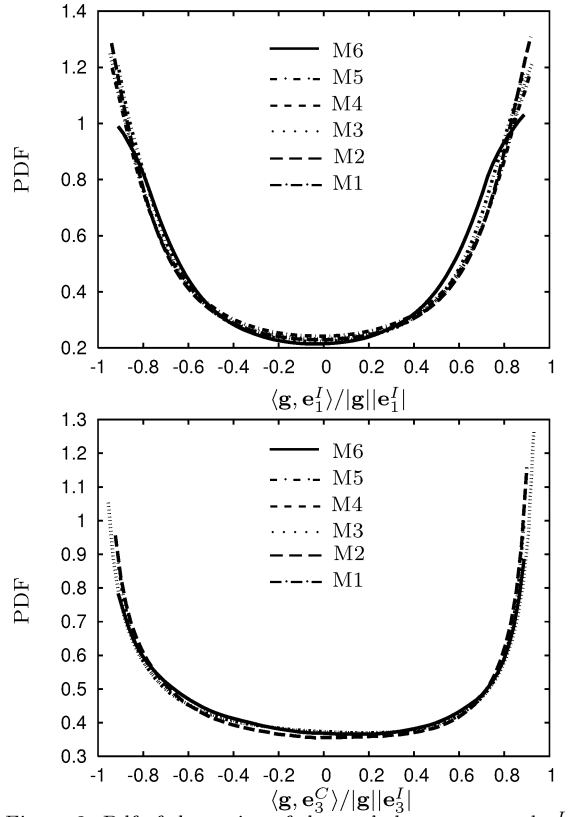

Figure 2: Pdf of the cosine of the angle between $\boldsymbol{g}$ and $\mathbf{e}_1^I$ (a), $\mathbf{e}_3^C$ (b).

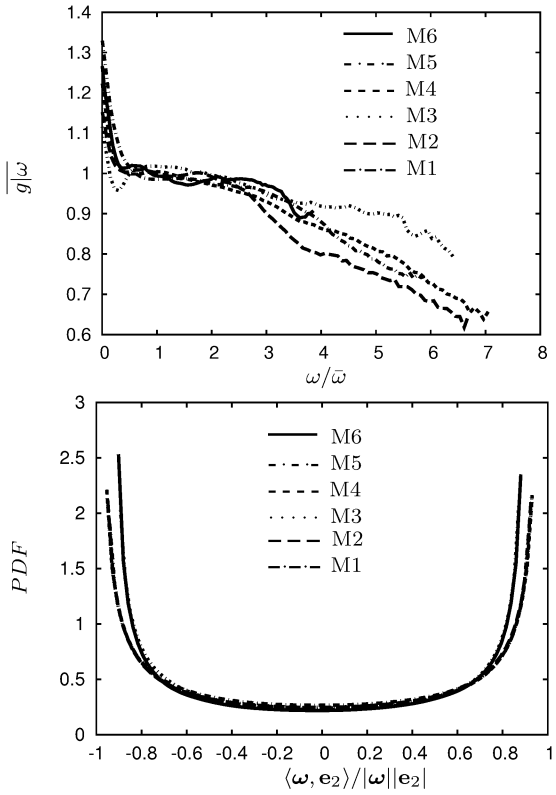

Figure 3: (a): $\mathbf{g}$ conditioned on $\omega = \sqrt{\omega_i \omega_i}$ (b): Pdf of the cosine of the angle between $\boldsymbol{\omega}$ and $\mathbf{e}_2$.

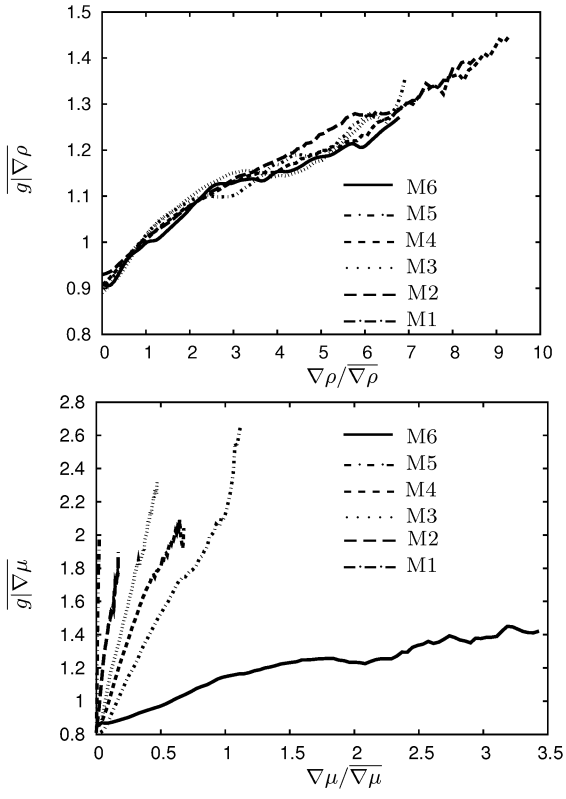

Figure 4: $\mathbf{g}$ conditioned on $\nabla\rho$ (a) and $\nabla\mu$ (b).

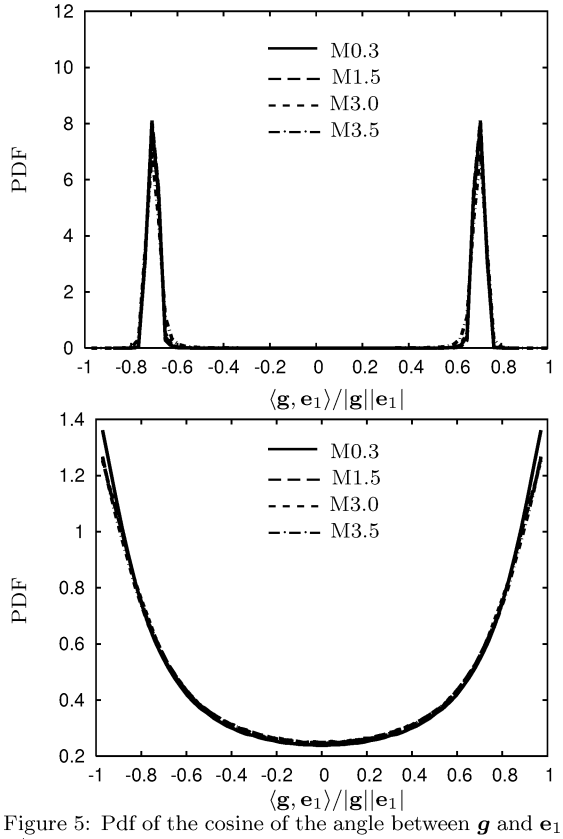

Figure 5: Pdf of the cosine of the angle between $\boldsymbol{g}$ and $\mathbf{e}_1$: (a) $x_2^+ = 6$, (b) $x_2/h = 1$.

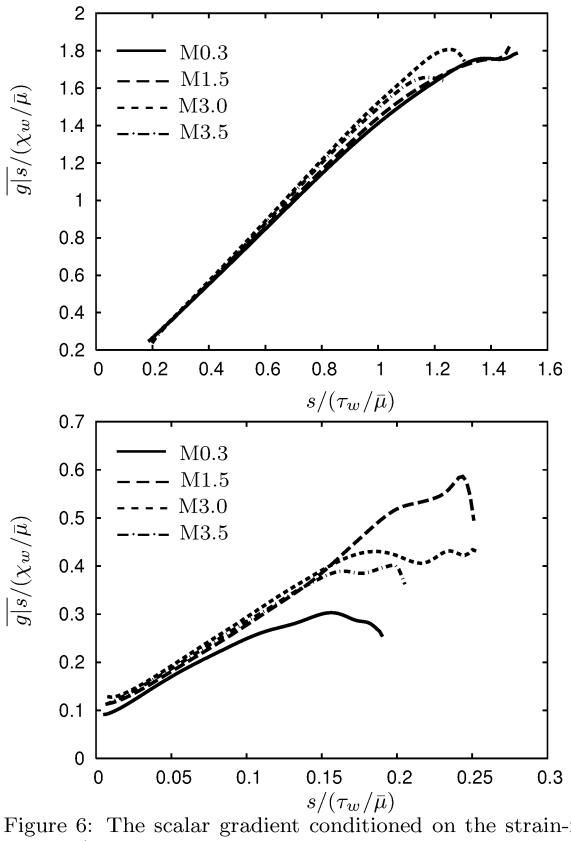

Figure 6: The scalar gradient conditioned on the strain-rate at (a):$x_2^+ = 6$, (b): $x_2/h = 1$, normalized by semilocal scalings (χ_w: scalar flux at the wall).

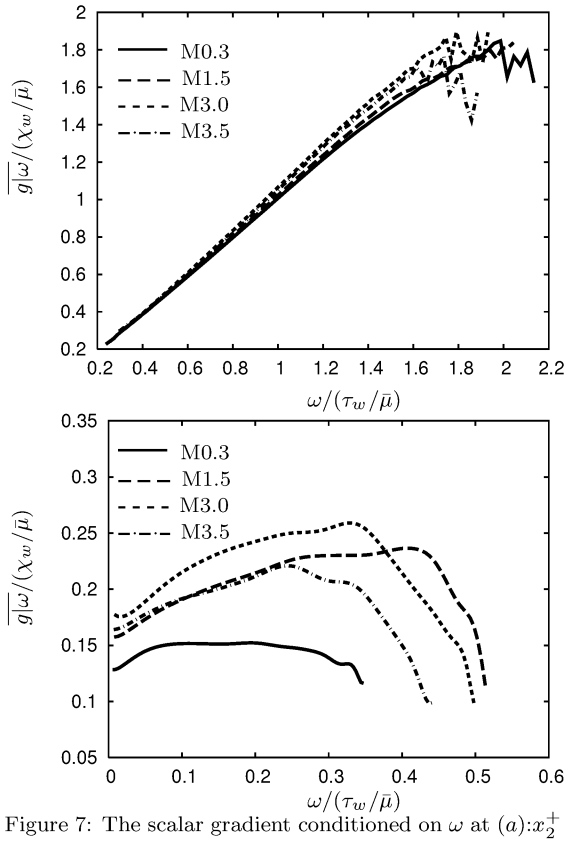

Figure 7: The scalar gradient conditioned on ω at (a):$x_2^+ = 6$, (b): $x_2/h = 1$, normalized by semilocal scalings (χ_w: scalar flux at the wall).

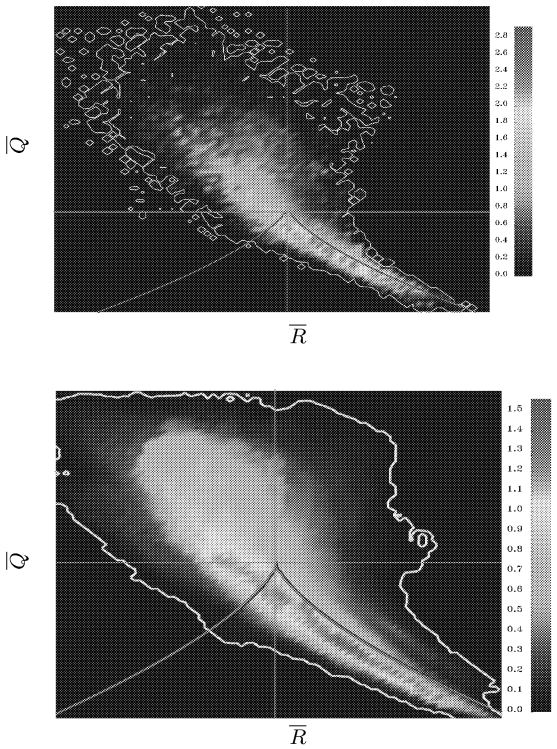

Figure 8: Scalar gradient conditioned on the second ($Q = -\frac{1}{2}A_{ij}A_{ji}$, with $A_{ij} = \frac{\partial u_i}{\partial x_j}$) and third invariant ($R = -\frac{1}{3}A_{ij}A_{jk}A_{ki}$). (a): $M_t = 0.05$ (b): $M_t = 0.63$.